Growth of Very Large MoS_2 Single Crystals Using Out-Diffusion Transport and Their Use in Field Effect Transistors

Sushil Kumar Pandey, *Member, IEEE*, Nezhueyotl Izquierdo, and Stephen A. Campbell, *Fellow, IEEE*

***Abstract*—Monolayer molybdenum disulfide (MoS_2) is an attractive 2D material with a wide range of potential applications in the field of electronics and optoelectronics. To obtain the best performance, it is very necessary to grow large area single crystals of MoS_2 (single domain) to avoid the effects of grain boundaries, but is exceptionally challenging to do this. Here, we report a novel method which we call out-diffusion vapor transport to grow large area single crystal monolayer MoS_2 using an otherwise conventional chemical vapor deposition system. In this method, microchannels were created on the boat to significantly limit the region where MoOx vapor can react with S vapor to form crystals. This growth method resulted in triangular monolayer MoS_2 single crystals up to $\sim$640 μm on a side grown on an oxidized silicon substrate, the largest crystals reported to date. Most of these crystals were multilayer at the center. This common feature has been identified in the literature as partially reduced transition metal oxide nucleates a second layer. We also achieved fully monolayer MoS_2 single crystals up to $\sim$450 μm on a side, the largest demonstrated without the MoOx. Fabricated field effect transistors (FET) using MoS_2 monolayer crystal as the active layer demonstrate a conventional n-type behavior, room-temperature mobility up to 45.5 $cm^2\ V^{-1}\ s^{-1}$ and a maximum ON-Current (ION) /OFF-current (IOFF) ratio of 1.8×10^7. Raman and Photoluminescence results indicate that the as-grown large area monolayer crystals have high crystalline quality and uniformity with minimal defects, a finding that is consistent with the high electron mobility. This research work provides a superior technique to grow large-area high-quality single-crystal monolayer MoS_2 without resorting to exotic equipment or techniques.**

***Index Terms*—2D materials, MoS_2, out-diffusion transport, chemical Vapor deposition, FET.**

I. Introduction

SINGLE crystals of two-dimensional transition metal dichalcogenides (TMDs) have drawn significant interest for their potential in the fields of novel electronic, optoelectronics, catalysis, lithium batteries, nanotribology, hydrogen storage and medical devices [1]–[12]. The most widely studied TMD, monolayer MoS_2, has the Mo layer sandwiched between two sulfur layers. As with most 2D materials, multilayer MoS_2 is held together by covalant forces. It too has generated considerable interest for field effect transistors (FETs), spin and valley devices, and photodetectors [4]–[12]. There are many technique for forming these materials such as micromechanical exfoliation, intercalation assisted exfoliation, liquid exfoliation, chemical vapor deposition (CVD), physical vapor deposition and hydrothermal synthesis, all of which have been employed to prepare monolayer MoS_2 [13]–[24]. The CVD methodology offers significant potential for inexpensive material production, making it a very attractive research target. Additionally, CVD has the capability for reproducibly fabricating high-quality large-area monolayer single crystals [19]–[23]. However, irrespective of precursor and growth recipe, the MoS_2 monolayer almost always consists of nonuniform separated triangular domains. The largest separate single triangular domain MoS_2 in the current literature is $\sim$350 μm [22]. Much larger polycrystalline monolayer MoS_2 films can be grown on a SiO_2 substrate, but crystalline grains are typically $<$20 μm [19]–[23]. As a result, domain boundaries produce low carrier mobility and degraded optical properties. It is noteworthy that Gong *et al.* and Chen *et al.* were able to grow large $MoSe_2$ crystals previously due to low reactivity of Se and optimized MoO_3 flux. But there is no report for growth of very large MoS_2 on SiO_2/Si substrate due to higher reactivity of S atoms than Se [25], [26]. Consequently, the growth of large MoS_2 single crystals (single domain) is strongly preferred.

Wei *et al.* reported MoS_2 separate single crystals with a largest size of $\sim$350 μm which were grown on a sapphire substrate [22]. In that work, O_2 was added to the Ar carrier gas to increase the crystal size. The process involves a delicate balance of oxidative etching of MoS_2 and MoS_2 growth. The best results only occur when the growth rate is slightly higher than the etch rate. This approach has several drawbacks. In the typical CVD process, material fluxes are difficult to control in part due to the nature of the volitization of fine grain powders where the surface area changes with time. Complicating the process further is the fact that the chalcogen flux comes from both the crucible and the tube walls, making the S flux even more variable. The second limitation is the extra amount of precursor needed and the need

Manuscript received October 1, 2020; revised March 10, 2021; accepted May 20, 2021. Date of publication May 25, 2021; date of current version June 22, 2021. This work was supported in part by National Science Foundation through the National Nano Coordinated Infrastructure (NNCI) program, Award # ECCS-1542202, and in part by the Characterization Facility, University of Minnesota, which receives partial support from National Science Foundation (NSF) through the Materials Research Science and Engineering Centers (MRSEC) program. *(Corresponding author: Stephen A. Campbell.)*

Sushil Kumar Pandey is working as Assistant Professor with the Department of Electronics and Communication Engineering, National Institute of Technology Karnataka, Surathkal, Mangalore 575025, India (e-mail: skpandey@nitk.edu.in).

Nezhueyotl Izquierdo and Stephen A. Campbell are with the Electrical and Computer Engineering Department, University of Minnesota, Minneapolis 55455 USA (e-mail: izqui007@umn.edu; campb001@umn.edu).

Digital Object Identifier 10.1109/TNANO.2021.3083686

for a large costly sapphire single crystal. Chi's group tried to control the MoO_3 flux using NiO foam which works as reactive barrier [27], but found that most of growth occurred at undesired top surface of substrate rather than surface facing the MoO_3 precursor through NiO foam [27]. The salt-assisted method was used to reduce the growth temperature of MoS_2, and in some cases create large crystals [28], [29], but the salt-assisted method has very high flux of precursors at substrate, resulting in a growth process that will change during the deposition and will be poorly controlled [28], [29]. Additionally, the chance of halide and alkali metal impurities is significant and the process must be tuned to the material chemistry.

Here, we report the growth of high-quality single grain monolayer MoS_2 crystals on an oxidized silicon substrate via the out-diffusion transport growth technique in a conventional CVD system. In this technique, microchannnels are first created on the edge of boat as shown by the light color (Fig. 1(a)). Next the substrates are placed upside down on the boat. The substrates covered about 85% of the boat area. While the transition metal boat is not fully enclosed, the geometry created a semi-confined cavity to better contain the MoO_x allowing for longer growth times for a fixed temperature and charge mass. It also creates a series of small, localized sources for the MoO_x vapor. It is at the exit of these microchannels that we can repeatedly find monolayer single crystals of MoS_2 with a maximum size of $\sim$450 μm and a room temperature electron mobility of 45.5 $cm^2/(V{\cdot}s)$.

II. Experimental Setup

A conventional tube-furnace CVD system was used to grow the MoS_2 single crystals. Microchannels were cut into the MoO_3 boat by hand using a sharp diamond cutter. The resultant channels were $\sim$300 μm deep, $\sim$400 μm wide, and $\sim$2.5 mm long (edge width of boat). The SiO_2/Si substrates were cleaned in a piranha solution (H_2SO_4: H_2O_2 = 4:1) and then dried at 150 °C, followed by a hexamethyldisilazane (HMDS) vapor treatment for five minutes. Immediately after the cleaning process, the SiO_2/Si substrates were properly aligned and placed facing down above a ceramic boat containing 1 mg of molybdenum oxide (MoO_3) powder (purity $\geq$99.5%) as shown in Fig. 1(b). A separate ceramic boat was loaded with 500 mg of sulfur (S) powder and placed upstream of the MoO_3 containing boat, at the edge of heating zone of the furnace.

After loading the boats and samples, the CVD system was purged with 500 sccm of ultra-high-purity Ar gas for 1 hour with the temperature set to at 100 °C. CVD growth took place at atmospheric pressure with 70 sccm of argon flowing in the tube. The furnace was then heated at a rate of 15 °C/min to 450 °C and held at that temperature for 15 min to allow the tube to stabilize. Then the temperature was ramped at 10 °C/min to the growth temperature and held at there for 20 min to allow growth. The growth temperature was varied from 700 to 850 °C. The temperature of the S boat was maintained at 350 °C during all growth processes by adjusting its distance from the main heating zone of the furnace. Once growth was complete, the furnace was cooled slowly (−10 °C/min) to 550 °C. Next, the Ar flow was increased to 500 sccm, the power was turned off, and the furnace was opened to quickly cool to 100 °C or below.

Microscopic images and the size of MoS_2 crystals were obtained with a high-resolution Keyence VHX5000 microscope. The thickness and surface image of MoS_2 monolayer crystals were achieved by a Bruker Nanoscope atomic force microscope (AFM) used in contact mode. Scanning electron microscopy was used to image the MoS_2 monolayer crystal. X-ray photoelectron spectroscopy with an Al Kα X-ray source was used to evaluate the elemental properties of MoS_2. An Auger Electron Spectroscopy system (PHI Model 670) was employed for 2D elemental mapping of MoS_2 crystals. Raman spectra and surface mapping of MoS_2 monolayers crystals were acquired using confocal Raman spectroscopy (WITec Alpha300R) with an Ar laser at 532 nm wavelength as the excitation source. The Raman spectroscopy system had a WITec (UHTS 300) detector. A 50X objective lens was used to focus the laser beam and to obtain the Raman signal. The spot size of the laser beam was 0.5 μm. The same laser and a different detector (WITec 2300i) were used to measure photoluminescence spectra and surface mapping.

MOSFET fabrication was performed using MoS_2 crystals grown directly on SiO_2/Si substrates. Optical lithography was used for device patterning. A Ti/Au (10/70 nm) stack was used as a contact pad for the source and drain regions. Next, the oxide was partially removed from back side by scratching with a diamond cutter. And silver (Ag) paste was used to contact the back of the wafer which served as the gate electrode. A Precision Semiconductor Parameter Analyzer (Hewlett Packard HP Agilent 4156A) was used to measure the electrical characteristics of the fabricated MoS_2 FETs. All electrical measurements were done at ambient conditions.

III. Results and Discussions

In agreement with previous work, we found that the monolayer MoS_2 crystal size increases with increasing MoO_3/substrate temperature. At 700 °C, no crystals were observed on the substrate area outside the boat (light color area of sample surface shown in Fig. 1(c)). This indicates that no out-diffusion of MoO_3 vapor at 700 °C (see Fig. 1(d)). It is noteworthy that there is negligible MoS_2 growth at the area of substrate above the microchannel. The continuous flow of MoO_3 precursor is believed to reduce the concentration of S vapor in this region. This reduces the chance of nucleation in the microchannels as shown in optical image of Fig. 1(c). There are nanoparticles/patches of MoO_x and Mo-O-S compounds on the substrate near both sides of microchannel and on the substrate between the microchannels. In this area the flux of both S vapor and MoO_x vapor are low. This promotes nucleation without significant growth. At 800 °C, the MoS_2 monolayer crystals start appearing, a few of them in range of 50–100 μm (see Fig. 1(d)). The density of crystals is large at this temperature. We found a huge increment in the crystal size upon further increasing temperature to 850 °C. In every sample it was observed that the largest crystals on the substrate were grown near the exit of the channel. Continuous films and multilayer crystals formed on the substrate directly above the boat. Fig. 1(c) is an SEM image of

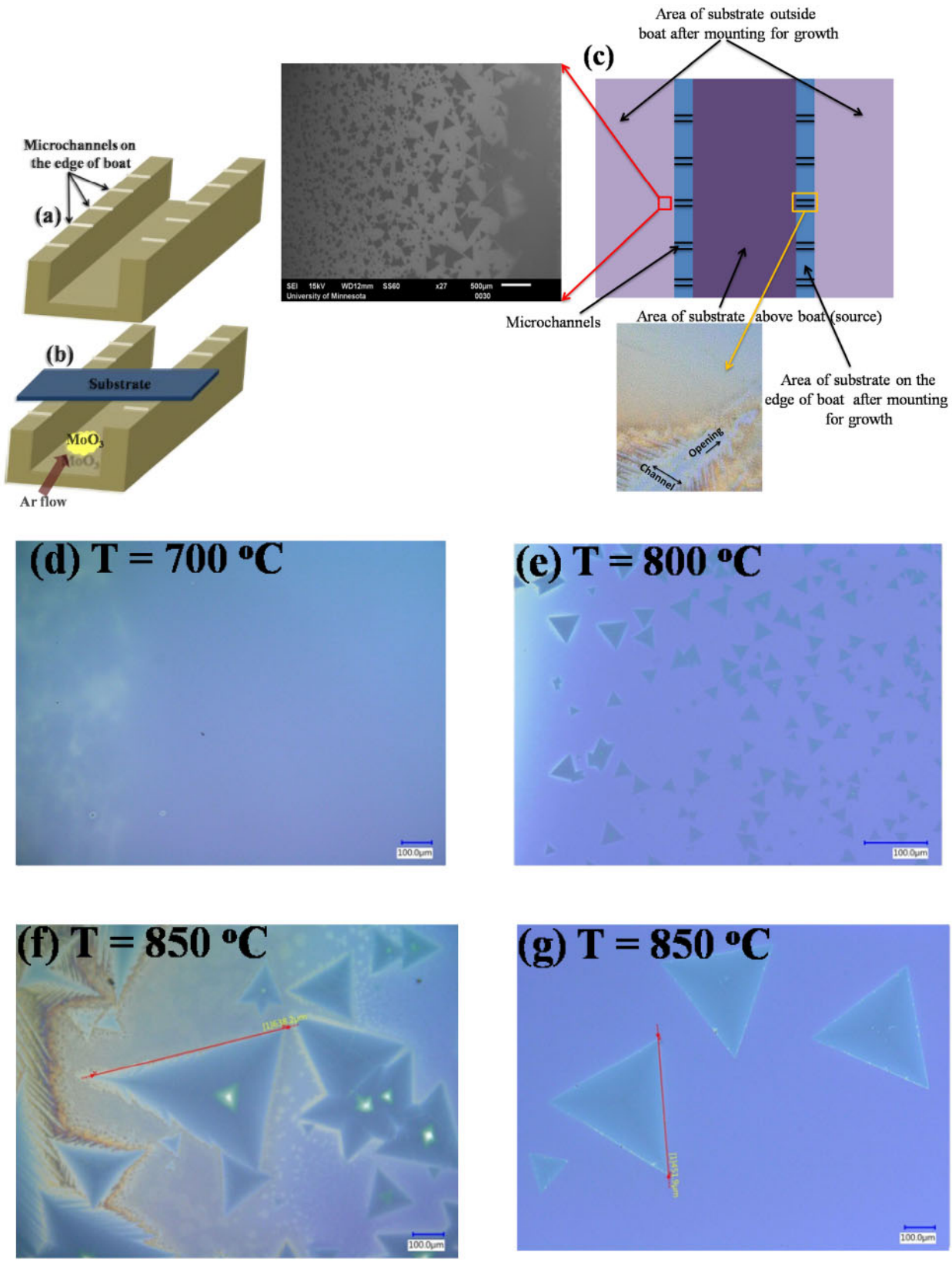

Fig. 1. Growth of monolayer MoS_2 large crystals on SiO_2/Si substrate. (a) Boat with microchannels, (b) Substrate mounted on boat having MoO_3 precursor, (c) Schematic of sample surface after growth, which has large crystals in the sample portion outside of the boat during growth. SEM image of marked portion is shown here indicating large crystals near edge of sizes close to 500 μm. Optical images of MoS_2 grown at temperature (d) 700 °C, (e) 800 °C, (f) 850 °C (close to the outside of the boat, which would have been just out of frame on the left side of the micrograph), and (g) 850 °C (further from the outside of the boat).

the surface area marked on the portion of sample just outside the microchannels during growth. The micrograph confirms large triangular monolayer MoS_2 crystal growth. We achieved the largest triangular crystals 640 μm on a side, however these had a small multilayer patch at the center as shown in Fig. 1(f). In Fig. 1(f), the nanoparticles/patches of Mo-O-S compounds impurities are covering the surrounding area of MoS_2 crystals. These nanoparticles/patches are formed due to partial reaction of MoO_x with sulfur during the growth. The thicknesses (height) of nanoparticles/patches are more than the monolayer MoS_2 thickness. Thus, MoS_2 looks lower than the surrounding surface, but in reality the MoS_2 crystal is above the substrate surface. We also got uniform monolayer crystals without a center patch of size 450 μm a small distance from the largest crystal on same sample surface as shown in Fig. 1(g). No one has heretofore reported a process that can produce such large crystals. The average size of monolayer crystals is $\sim$372 μm which is calculated considering the substrate area outside the boat from microchannel exit point (typically $\sim$0.5 cm $\times$ $\sim$2 cm).

The incommensurate growth of 2D materials, like most other materials, can be divided into nucleation and growth. Nucleation centers of transition metal dichalcogenides grown from metal oxide and chalcogen powders are typically ascribed to be suboxides of the transition metal source. The density of these centers plays a key role in the ultimate deposition. In a typical vapor transport process such as this, the flux of the metal suboxide depends critically on the temperature of the source and the flux of the reducing agent, in this case, sulfur. The continuous film on the substrate inside the boat suggests a very high nucleation density in that region. The distribution of large crystals suggests a much lower nucleation immediately outside of the microchannel, dropping further as the distance from the channel exit increases, either axially or radially. In our out-diffusion transport technique, the pressure difference is not sufficient to drive the flow of gas through the microchannels. Instead the MoO_x vapor diffuses through the channels, driven by the concentration gradient created by crystal growth. Also, due to the large surface area, it is likely that a significant amount of MoO_x will adsorb on the walls of the microchannel. This gettering effect would reduce the MoO_x flux exiting the microchannel during growth initiation, decreasing the nucleation density. As the microchannel surfaces become saturated, the MoO_x flux may increase, permitting faster growth. If same boat is used in multiple growths runs (at same growth parameters) without micro-channels cleaning, the crystals size decreases slowly with increase in number of runs due to a reduction in the effective size (especially width and depth) of microchannel by adsorbed MoO_x on the walls.

Growth depends on the flux of the two species and the thermodynamics of the growth process at the substrate temperature. The shape of the crystal is determined by the growth rate of various crystal faces. The faces with the fastest growth rates may become smaller or disappear, while the slowest growing faces generally emerge as the largest [21]–[31]. The growth rate of these faces is influenced by the surface free energy which corresponds to edge free energy in case of 2D crystals [21]–[31]. The low-energy faces have a tendency to grow slowly. In case of monolayer MoS_2, most of the obtained edge terminations are Mo zigzag (Mo-zz) and S zigzag (S-zz) because of their energetically stable structures [21]–[31]. The final shape of MoS_2 crystals is decided by the growing rate of different edge terminations. Both of these terminations have zigzag edges. In S-zz and Mo-zz edges terminations, the S atoms and Mo atoms are exposed to the outside, respectively.

MoS_2 domains for all shapes begin growing from a hexagonal nucleus that has three edges of Mo-zz terminations and remaining three edges of S-zz terminations. The microchannels cause the Mo to S flux ratio to be much less than one, resulting in S-zz edge terminated growth. Due to the excess of S, the growth rate is proportional to the MoO_x arrival flux. In this S rich growth condition, Mo-zz terminations grow quicker compared to the S-zz terminations, simply because in S adequate ambiance, Mo-zz terminations with unsaturated Mo atoms exposed to the outside are more energetically unstable than the S-zz terminations, and so have a larger likelihood of interacting and bonding with free S atoms. Since Mo-zz terminations grow faster, the domain shape changes from a hexagon to a triangle with three edges of S-zz terminations [21]–[31].

The key to forming large triangular crystals in 2D growth is controlling the flux of the deficit species, in this case the MoO_x exiting the microchannels. Since solid sources invariably have poor flux control, it is often best to provide a method for producing a flux gradient, reasoning that this will produce a range of growth conditions, some of which will produce large crystals. Once the vapor exits the microchannel it encounters the S vapor allowing further reduction. It also diffuses both vertically and laterally, and is pushed laterally by the carrier gas flow. Of course, the geometry of the boat and substrate create a boundary layer that limits the effect of Ar flow close to the surface. In the regions close to the exterior of the microchannels but on the substrate that the conditions favor the growth of large crystals.

The above explanation can also be expressed as follows. The exit point of microchannels behaves as source of MoO_x vapor which diffuses on the substrate area outside the boat. The MoO_x vapor concentration then decreases with distance from the source (exit point of microchannel). Additionally, once the MoO_x vapor exits the microchannel it encounters S vapor. The resulting chemical reactions for growth of MoS_2 further depletes the MoO_x. Since the nucleation probability is a function of the MoO_x vapor concentration, the nucleation density decreases with increase in distance from the microchannel exit point. Since the deposition was done in excess S vapor, its concentration is nearly uniform, but the MoO_x vapor concentration decreases with distance, indicating higher reaction rate (growth rate) near microchannel exit point than reaction rate away from microchannel exit point. Therefore, the growth rate also decreases with increased distance from microchannel exit point. Finally, near the exit point of microchannel, the growth rate is high and nucleation density is average, conditions that support the growth of very large MoS_2 crystals.

From the atomic force microscopy (AFM), we observe the smooth surface morphology of a MoS_2 monolayer crystal (Fig. 2(a)). The image is produced by scanning near the edge of a large crystal. The cross sectional height profile reveals that the thickness of the MoS_2 crystal is $\sim$0.89 nm (Fig. 2(b)), which is

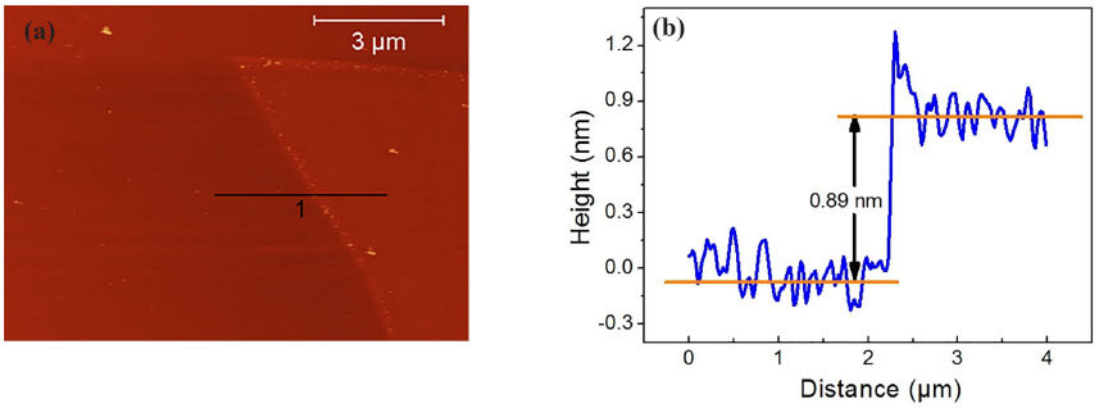

Fig. 2. (a) AFM image and (b) height profile for an MoS_2 crystal (scanned near the edge of crystal) taken across the black line in fig. 2(a).

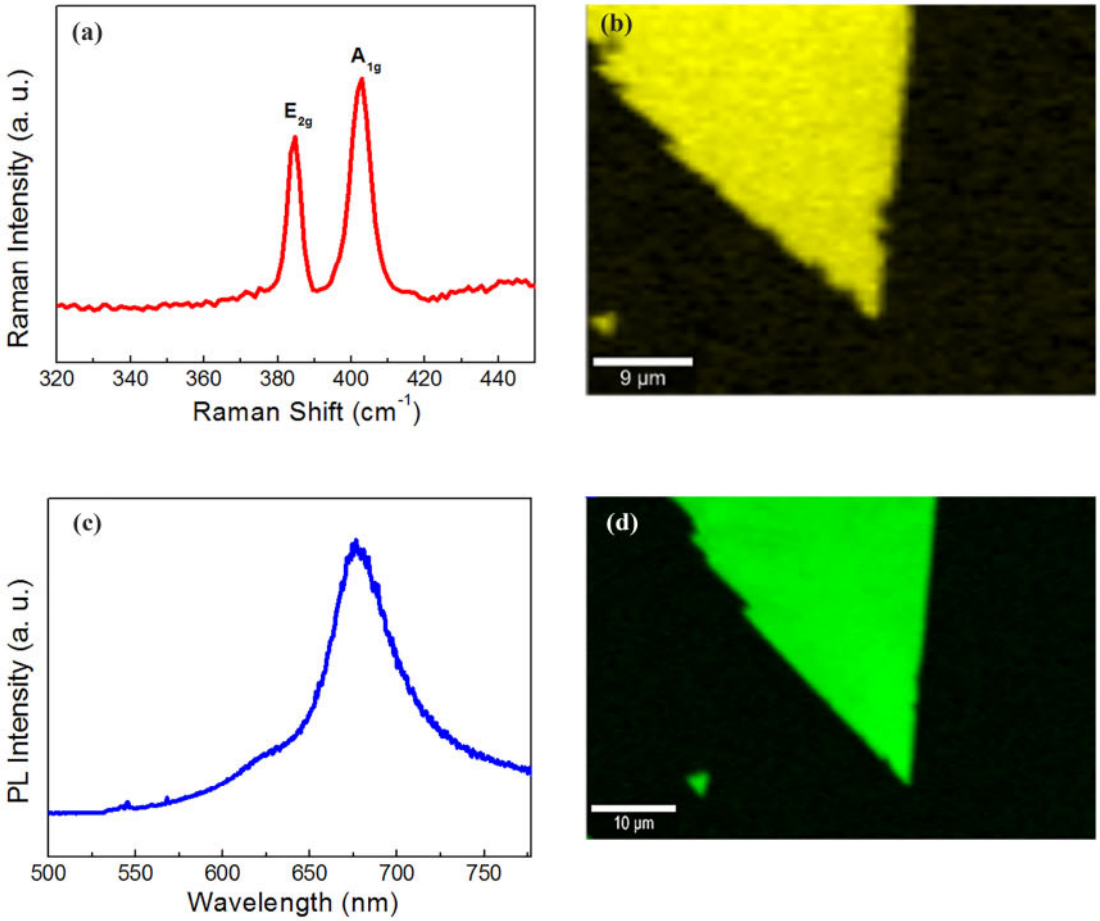

Fig. 3. (a) Raman spectrum, (b) 2D image of spatial variation of the magnitude of the frequency difference between A_{1g} and E_{2g} in Raman measurement of the edge of a triangular MoS_2 crystal, (c) PL spectrum of an MoS_2 crystal, (d) 2D images of the PL intensity of the edge of a triangular MoS_2 crystal.

consistent with a monolayer crystal as reported earlier for MoS_2 on a SiO_2/Si substrate [32].

We observed two vibration modes, E_{2g} and A_{1g}, in the Raman spectra of the MoS_2 monolayer crystal. The E_{2g} mode is generated by the in-plane vibration of molybdenum and sulfur atoms whereas the A_{1g} mode corresponds to the out-of-plane vibration of sulfur atoms [33]. The E_{2g} and A_{1g} modes are located at 384.41 and 402.78 cm^{-1}, respectively, resulting a frequency difference Δk of 18.37 cm^{-1} shown in Fig. 3(a). This frequency difference value agrees with the value obtained for monolayer MoS_2 as reported previously [31]–[33]. The E_{2g} peak has a full width at half-maximum of value 3.82 cm^{-1}, very close to value of 3.7 cm^{-1} obtained for exfoliated monolayer MoS_2 [33]–[35], indicating good crystalline quality of monolayer crystals grown by CVD out-diffusion transport. Additionally, Raman mapping was performed near the edge of a large triangular MoS_2 crystal as shown in Fig. 3(b) where the two-dimensional spatial variation of the magnitude of difference between A_{1g}

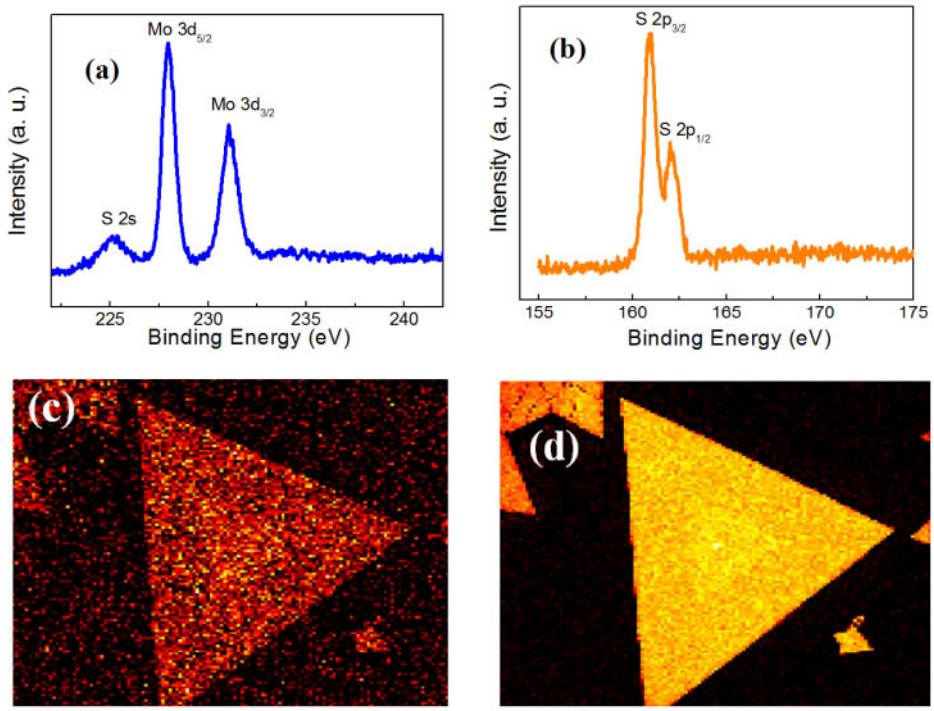

Fig. 4. XPS spectrum of (a) Mo 3*d* and S 2*s*, (b) S 2*p* binding energy peaks from the MoS_2 crystal on the SiO_2/Si substrate. Auger elemental map of (c) Mo and (d) S from the MoS_2 crystal on the SiO_2/Si substrate.

and E_{2g} peaks were plotted. The uniform color intensity of image indicates the thickness uniformity of monolayer MoS_2 crystal.

Photoluminescence (PL) spectroscopy was been performed for the MoS_2 monolayer crystals as shown in Fig. 3(c). A prominent PL peak at 676 nm wavelength was observed. This corresponds to the emission from A1 direct excitonic transitions [36]. The broad peak at ∼625 nm is due to B1 direct excitonic transitions [36]. Additionally, the 2D images of the PL intensity for MoS_2 crystal has been measured by stepping a focused excitation laser (532 nm) near edge of crystal and integrating the PL signal from each point as shown in Fig. 3(d). These results related to PL measurement indicate high crystallinity (insignificant defect formation) and thickness uniformity of the MoS_2 monolayer crystals [36]–[38].

Selected area X-ray photoelectron spectroscopy (XPS) was used to examine the stoichiometry of MoS_2 monolayer crystals. All XPS spectra were corrected against the C 1s carbon peak at 284.8 eV to compensate for sample charging during measurement. We observed the core level binding energies of Mo^{4+} $3d_{5/2}$ and $3d_{3/2}$ doublet peaks at 229.5 and 232.6 eV, respectively as shown in Fig. 4(a) [39]–[41]. These binding energy peaks of Mo-3d indicate stoichiometric intrinsic MoS_2 which has a minimal concentration of defects such as sulfur vacancies [39]–[41]. There is a negligible concentration of Mo^{6+} states at 236.0 eV, indicating no evidence of MoO_3 suboxides. This matches the results obtained by PL and Raman mapping measurement. The sulfur (S) 2s, $2p_{3/2}$ and $2p_{1/2}$ peaks were located at 226.6, 160.9 and 162.1 eV respectively suggests the charge state of S^{2-} as shown in Fig. 4(a,b) [39]–[41]. The extrapolated S/Mo atomic ratio was ≈2.0 for the large MoS_2 crystals indicating good stoichiometry. Auger electron spectroscopy (AES) was also performed to confirm the material composition of triangular shaped monolayer crystals. Micro-area Auger mapping of elements Mo and S as shown in Figs 4(c) and (d) respectively, determined that the triangle crystals consist of Mo and S atoms thus indicating MoS_2. The AES electron spectra demonstrated that the relative atomic ratios of the Mo and S were consistent with a fully stoichiometric (1:2) monolayer layer [42].

To measure the electrical properties of the grown MoS_2 monolayer crystals, back-gated field-effect transistors (FET) using MoS_2 crystal grown on a 250 nm thick thermal SiO_2 grown on a (100) p-type Si substrate was fabricated employing standard optical photolithography processes (see Fig. 5 (a) and (b)). A Ti/Au metal (10/70 nm) stack was used as a contact pad for the source and drain regions. Ag paste was used to contact the back of the wafer, which served as the gate electrode (see Fig. 5(a)). The estimated length and width of the channel of this FET are ∼30 μm and ∼160 μm respectively. The output and transfer characteristics of this fabricated device are demonstrated in Fig. 5 (c) and (d), respectively. These transistor characteristics were measured under ambient conditions to find the on/off ratio, threshold voltage, and carrier mobility. The latter two parameters were extracted from the drain to source current (I_{DS}) versus the gate voltage (V_G) transfer characteristics. The devices demonstrate distinctive n-type behavior. The achievement of a linear segment of I_{DS} vs drain to source voltage (V_{DS}) curve under low bias conditions, indicates an ohmic-like contact at the source and drain.

We observed a maximum ratio of 1.8×10^7 for on-current (I_{ON}) to off-current (I_{OFF}) at room temperature. The threshold voltage for this device is 20.5 V as calculated by linear extrapolation method using Fig. 5(d). The calculation of field-effect

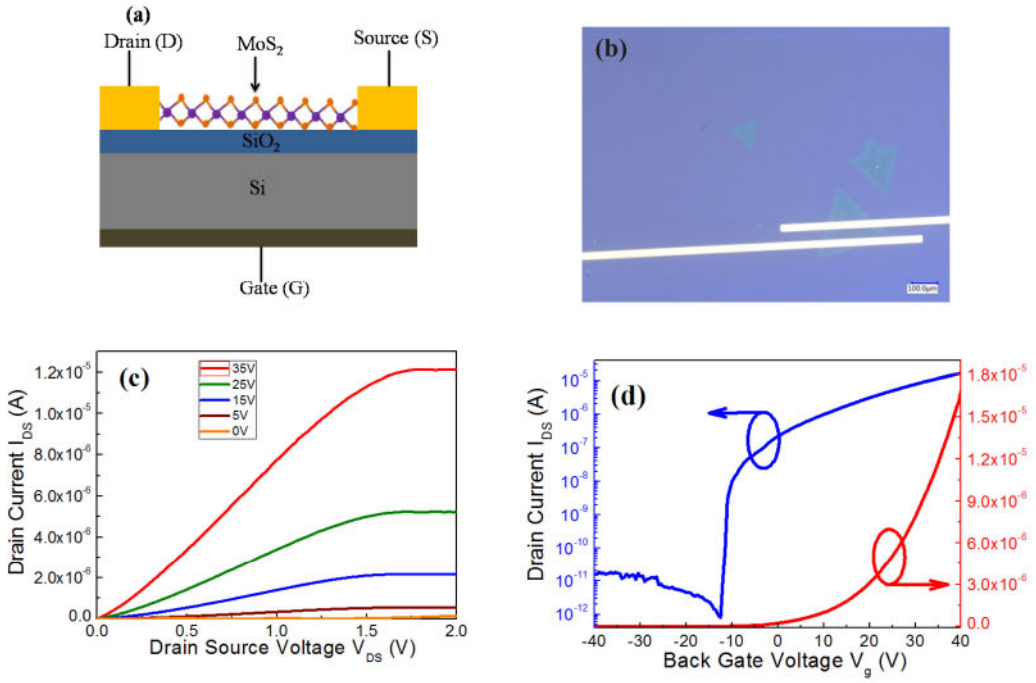

Fig. 5. (a) Schematic of the monolayer MoS_2 FET device structure. (b) Optical image of fabricated FET structure (top view) having device channel length ~30 μm. (c) Output characteristics of the device at different gate voltages. (d) Transfer characteristics of the device with variable gate voltage.

mobility of electrons was performed using the slope $\Delta I_{DS}/\Delta V_G$ fitted to the linear regime of the transfer (I_{DS}-V_{GS}) curve. The formula employed was $\mu = (L/WC_{ox}V_{DS})(\Delta I_{DS}/\Delta V_G)$, where L, W and C_{ox} are the channel length, width and gate capacitance per unit area respectively. The electron mobility of MoS_2 monolayer crystal device was found to be as high as 45.5 cm^2 / (V·s) in ambient, in agreement with earlier studies for an exfoliated or CVD grown MoS_2 crystals [7], [8]. In MoS_2 monolayers, a reduction of electron mobility is primarily due to presence of sulfur vacancies which can trap electrons and so act as charged scattering centers [43], [44]. The high electron mobility of our grown MoS_2 crystals signifies a relatively low sulfur vacancy concentration which can be justified by the high sulfur vapor condition during our growth. These kinds of outcomes suggest that our large-area MoS_2 crystals are comparable to some of the best MoS_2 reported.

IV. Conclusion

In summary, we report the growth of large triangular single-crystal domains monolayer directly on SiO_2/Si substrates using an out-diffusion method in a standard CVD system. We observe triangular single-crystal MoS_2 domains with side lengths of up to ~640 μm, the largest reported to date on SiO_2/Si substrates. The Raman and Photoluminescence mapping results confirm the uniform surfaces of the grown large area monolayer crystals. XPS and Auger spectroscopy measurements indicate good stoichiometry of the large area monolayer MoS_2 crystals. Back-gated FETs made with these MoS_2 monolayer crystals show n-type behavior having a turn-on voltage 20.5 V and a maximum on/off ratio as high as 1.8×10^7. Our developed growth method is capable of growing high-quality large MoS_2 domains which offer a potential material platform for electronic and optoelectronic devices applications.

References

[1] R. Tenne, L. Margulis, M. Genut, and G. Hodes, "Polyhedral and cylindrical structures of tungsten disulphide," *Nature*, vol. 360, pp. 444–446, 1992.
[2] L. Margulis, G. Salitra, M. Talianker, and R. Tenne, "Nested fullerene-like structures," *Nature*, vol. 365, pp. 113–114, 1993.
[3] Y. Feldman, E. Wasserman, D. J. Srolovitz, and R. Tenne, "High-rate, gas-phase growth of MoS_2 nested inorganic fullerenes and nanotubes," *Science*, vol. 267, no. 5195, pp. 222–225, 1995.
[4] R. Tenne, "Doped and heteroatom-containing fullerene-like structures and nanotubes," *Adv. Mater.*, vol. 7, no.12, pp. 965–995, 1995.
[5] Y. Golan, C. Drummond, M. Homyonfer, Y. Feldman, R. Tenne, and J. Israelachvili, "Microtribology and direct force measurement of WS_2 nested fullerene-like nanostructures," *Adv. Mater.*, vol. 11, no.11, pp. 934–937, 1999.
[6] M. Chhowalla, and G. A. Amaratunga, "Thin films of fullerene-like MoS_2 nanoparticles with ultra-low friction and wear," *Nature,* vol. 407, pp. 164–167, 2000.
[7] B. Radisavljevic, A. Radenovic, J. Brivio, V. Giacometti, and A. Kis, "Single-layer MoS_2 transistors," *Nat. Nanotechnol.*, vol. 6, pp. 147–150, 2011.
[8] H. Schmidt *et al.*, "Transport properties of monolayer MoS_2 grown by chemical vapor deposition," *Nano Lett.*, vol. 14, no. 4, pp. 1909–1913, 2014.
[9] H. Zeng, J. Dai, W. Yao, D. Xiao, and X. Cui, "Valley polarization in MoS_2 monolayers by optical pumping," *Nat. Nanotechnol.*, vol. 7, pp. 490–493, 2012.
[10] K. F. Mak, K. L. McGill, J. Park, and P. L. McEuen, "The valley hall effect in MoS_2 transistors," *Science*, vol. 344, no. 6191, pp. 1489–1492, 2014.
[11] Z. Yin *et al.*, "Single-layer MoS_2 phototransistors," *ACS Nano*, vol. 6, no. 1, pp. 74–80, 2012.
[12] O. Lopez-Sanchez, D. Lembke, M. Kayci, B. Radenovic, and A. Kis, "Ultrasensitive photodetectors based on monolayer MoS_2," *Nat. Nanotechnol.*, vol. 8, pp. 497–501, 2013.

[13] H. Li *et al.*, "Fabrication of single- and multilayer MoS_2 film-based field-effect transistors for sensing NO at room temperature," *Small*, vol. 8, no. 1, pp. 63–67, 2012.
[14] K. G. Zhou, N. N. Mao, H. X. Wang, Y. Peng, and H. L. Zhang, "A mixed-solvent strategy for efficient exfoliation of inorganic graphene analogues," *Angew. Chem.,* vol. 50, no. 46, pp. 10839–10842, 2011.
[15] Z. Zeng *et al.*, "Single-Layer semiconducting nanosheets: High-yield preparation and device fabrication," *Angew. Chem.,* vol. 50, no. 47, pp. 11093–11097, 2011.
[16] C. N. R. Rao, and A. Nag, "Inorganic analogues of graphene," *Eur. J. Inorg. Chem.,* vol. 2010, no. 27, pp. 4244–4250, 2010.
[17] C. Gong *et al.*, "Metal contacts on physical vapor deposited monolayer MoS_2," *ACS nano*, vol. 7, no. 12, pp. 11350–11357, 2013.
[18] [18] S. Wu, C. Huang, G. Aivazian, J. S. Ross, D. H. Cobden and X. Xu, "Vapor–solid growth of high optical quality MoS_2 Monolayers with near-unity valley polarization,"*ACS Nano,* vol. 7, no. 3, pp. 2768–2772, 2013.
[19] C. B. L. Posadas, Y. Wei, W. Shen, D. Kahr, M. Hohage, and L. Sun, "Direct observation of the CVD growth of monolayer MoS_2 using in situ optical spectroscopy," *Beilstein J. Nanotechnol.*, vol. 10, pp. 557–564, 2019.
[20] M. Ardahe, M. R. Hantehzadeh, and M. Ghoranneviss, "Effect of growth temperature on physical properties of MoS_2 Thin films synthesized by CVD," *J. Electron. Mater.,* vol. 49, pp. 1002–1008, 2020.
[21] S. Wang *et al.*, "Shape evolution of monolayer MoS_2 Crystals grown by chemical vapor deposition," *Chem. Mater.*, vol. 26, no. 22, pp. 6371–6379, 2014.
[22] W. Chen *et al.*, "Oxygen-assisted chemical vapor deposition growth of large single crystal and high-quality monolayer moS_2," *J. Amer. Chem. Soc.,* vol. 137, no. 50, pp. 15632–15635, 2015.
[23] Y. H. Lee *et al.*, "Synthesis of large-area MoS_2 atomic layers with chemical vapor deposition," *Adv. Mater.,* vol. 24, no. 17, pp. 2320–2325, 2012.
[24] D. Wu *et al.*, "Epitaxial growth of highly oriented metallic MoO_2@MoS_2 Nanorods on C-Sapphire," *J. Phys. Chem. C*, vol. 122, no. 3, pp. 1860−1866, 2018.
[25] Y. Gong *et al.*, "Synthesis of millimeter scale transition metal dichalcogenides single crystals," *Adv. Funct. Mater.*, vol. 26, no. 12, pp. 2009–2015, 2016.
[26] J. Chen *et al.*, "Chemical vapor deposition of large-size monolayer $MoSe_2$ Crystals on molten glass," *J. Amer. Chem. Soc.*, vol. 139, no. 3, pp. 1073−1076, 2017.
[27] Y. F. Lim *et al.*, "Modification of vapor phase concentrations in MoS_2 growth using a NiO foam barrier," *ACS Nano*, vol. 12, no. 2, pp. 1339−1349, 2018.
[28] J. Zhou, J. Lin, and X. Huang, " A library of atomically thin metal chalcogenides," *Nature*, vol. 556, pp. 355–359, 2018.
[29] Y. Jin *et al.*, "Na_2SO_4-Regulated high-quality growth of transition metal dichalcogenides by controlling diffusion," *Chem. Mater.*, vol. 32, no. 13 pp. 5616–5625, 2020.
[30] J. J. De Yoreo, P. G. Vekilov, P. M. Dove, and S. Weiner, "Biomineralization: Review in mineralogy and geochemistry," *Mineralogical Soc. Amer. Geochemical Soc.: Chantilly,* vol. 4, no. 1, pp. 81–82, 2003.
[31] Y. H. Lee *et al.*, "Synthesis and transfer of single-layer transition metal disulfides on diverse surfaces," *Nano Lett.,* vol. 13, no. 4, pp. 1852–1857, 2013.
[32] C. Lee, H. Yan, L. E. Brus, T. F. Heinz, J. Hone, and S. Ryu, "Anomalous lattice vibrations of single- and few-layer MoS_2," *ACS Nano*, vol. 4, no. 5, pp. 2695–2700, 2010.
[33] P. Tonndorf *et al.*, "Photoluminescence emission and raman response of monolayer MoS_2, $MoSe_2$, and WSe_2," *Opt. Exp.,* vol. 21, no. 4, pp. 4908–4916, 2013.
[34] Y. Yu, C. Li, Y. Liu, L. Su, Y. Zhang, and L. Cao, "Controlled scalable synthesis of uniform, high-quality monolayer and few-layer MoS_2films," *Sci. Rep.*, vol. 3, pp. 18661–18666, 2013.
[35] X. Ling *et al.*, "Role of the seeding promoter in MoS_2 Growth by chemical vapor deposition," *Nano Lett,* vol. 14, no. 2, pp. 464–472, 2014.
[36] C. W. Lee *et al.*, "Toward high-performance solution-processed carbon nanotube network transistors by removing nanotube bundles," *J. Phys. Chem. C*, vol. 112, no. 32, pp. 12089–12091, 2008.
[37] K. F. Mak, C. Lee, J. Hone, J. Shan, and T. F. Heinz, "Atomically thin MoS_2: A new direct-gap semiconductor," *Phys. Rev. Lett,* vol. 105, no. 13, pp. 1368051–1368054, 2010.
[38] A. Splendiani *et al.*, "Emerging photoluminescence in monolayer MoS_2," *Nano Lett.*, vol. 10, no. 4, pp. 1271–1275, 2010.
[39] Y. Zhan, Z. Liu, S. Najmaei, P. M. Ajayan, and J. Lou, "Large-area vapor-phase growth and characterization of MoS_2 Atomic layers on a SiO_2 Substrate," *Small*, vol. 8, no. 7, pp. 966–971, 2012.
[40] J. Mann *et al.*, "Facile growth of monolayer MoS_2 film areas on SiO_2," *Eur. Phys. J. B,* vol. 86, pp. 2261–2264, 2013.
[41] M. Donarelli, F. Bisti, F. Perrozzi, and L. Ottaviano, "Tunable sulfur desorption in exfoliated MoS_2 by means of thermal annealing in ultra-high vacuum," *Chem. Phys. Lett.*,vol. 588, pp. 198–202, Nov. 11, 2013.
[42] P. Joensen, E. D. Crozier, N. Alberding, and R. F. Frindt, "A study of single-layerand restacked MoS_2 by X-ray diffraction and X-ray absorption spectroscopy," *J. Phys. C: Solid State Phys.*, vol. 20, no. 26, pp. 4043–4053, 1987.
[43] W. Zhou *et al.*, "Intrinsic structural defects in monolayer molybdenum disulfide," *Nano Lett.,* vol. 13, no. 6, pp. 2615–2622, 2013.
[44] W. Zhu *et al.*, "Electronic transport and device prospects of monolayer molybdenum disulphide grown by chemical vapour deposition," *Nat. Commun.,* vol. 5, pp. 30871–30878, 2014.